Microstructure/Mechanical Property Relationships of Submerged Arc Welds in HSLA 80 Steel

Submerged arc welds made at various energy inputs are evaluated in terms of microstructure and mechanical properties, in both as-welded and stress-relieved conditions

BY N. J. SMITH, J. T. McGRATH, J. A. GIANETTO AND R. F. ORR

ABSTRACT. The relationship between microstructure and mechanical properties was examined for weld metal and heat-affected zones of submerged arc welds deposited in HSLA 80 steel. The welds, deposited over an energy input range of 2–4 kJ/mm (51–102 kJ/in.) with two commercial consumable combinations, exceeded the targeted notch toughness properties in the as-welded condition. The superior toughness resulted from a high proportion of acicular ferrite and low ($O + S \leq 0.031$) content. The notch toughness of the coarse-grain heat-affected zone (CGHAZ) decreased with increasing energy input. The low toughness at the highest (4 kJ/mm) energy input resulted from the increased proportion of CGHAZ taking part in the fracture and the formation of a coarse upper bainite microstructure. Stress relieving reduced the notch toughness of both the weld metal and heat-affected zone as a result of embrittlement caused by carbide precipitation and an increase in yield strength resulting from copper precipitation.

KEY WORDS

As-Welded Properties
Mechanical Properties
Stress Relieved
SA Welds in HSLA 80
Submerged Arc Welds
2–4 kJ/mm Energy Input
Coarse-Grain HAZ
Notch Toughness
Copper Precip. Steel
Cu Precip. Hardening

N. J. SMITH, J. T. McGRATH, J. A. GIANETTO and R. F. ORR are with Metals Technology Laboratories (formerly Physical Metallurgy Research Laboratories), CANMET, Ottawa, Ont., Canada.

Paper presented at the 69th Annual AWS Meeting, held April 17-22, 1988, in New Orleans, La.

Introduction

Current interest in the fabrication of naval surface ships and submarines has prompted renewed studies on submerged arc welding of conventional high-strength quenched-and-tempered (Q&T) steels, particularly HY 80 (Ref. 1) and HY 100 (Ref. 2). Recently, several papers have been published on the development of copper-precipitation-strengthened steels that have potentially the same (or better) strength and toughness properties, with improved weldability compared to the conventional Q&T steels (Refs. 3–5). One of these steels, designated HSLA 80, is a modified version of ASTM A710 Grade A Class 3, and is currently being specified for the construction of U.S. Navy ships (Ref. 6).

HSLA 80 steel differs from the conventional higher-carbon quenched-and-tempered HY steels in that the strength is obtained through copper precipitation hardening. The steel has lower carbon and alloy levels, and therefore does not transform to the hard martensitic structure associated with the HY steels. This leads to improved weldability and essentially eliminates the need for preheating at ambient temperatures above 0°C (32°F). However, only limited published research exists on the evaluation of weldability and mechanical properties of weldments in ASTM A710 (Refs. 7, 8) and HSLA 80 (Refs. 9–11). The recent work of Jesseman and Schmid (Ref. 7) focused on the evaluation of copper-containing steels (ASTM A710 Grade A and ASTM A736), with the aim of determining the effects of base plate heat treatment class, welding energy input, and plate thickness-heat flow conditions on the HAZ toughness and hardness. They also reported weld metal properties for several welding consumable combinations for both the as-welded and PWHT conditions. However, in order to establish the suitability of the HSLA 80 steel for critical applications and to provide guidance with regard to welding procedure development, there is a need for further research to obtain more quantitative results on structure/property relationships of weld metals and heat-affected zones. The objective of the present study was to perform a quantitative analysis of the microstructure/mechanical property relationships of submerged arc welds deposited in low-carbon, copper-precipitation-strengthened HSLA 80 steel.

Experimental

Base Material and Welding Procedure

Microstructure and mechanical property studies were performed on experimental submerged arc welds deposited in 25.4-mm (1-in.) thick HSLA 80 steel, the composition of which is listed in Table 1. The mechanical property requirements presented in Table 2 were established from current military standards concerned with the qualification of sub-

Table 1—Chemical Composition of HSLA 80 High-Strength Steel

Element, wt-%										
C	Mn	Si	S	P	Ni	Cr	Mo	Cu	V	Nb
0.060	0.50	0.27	0.004	0.007	0.92	0.66	0.25	1.02	0.005	0.044

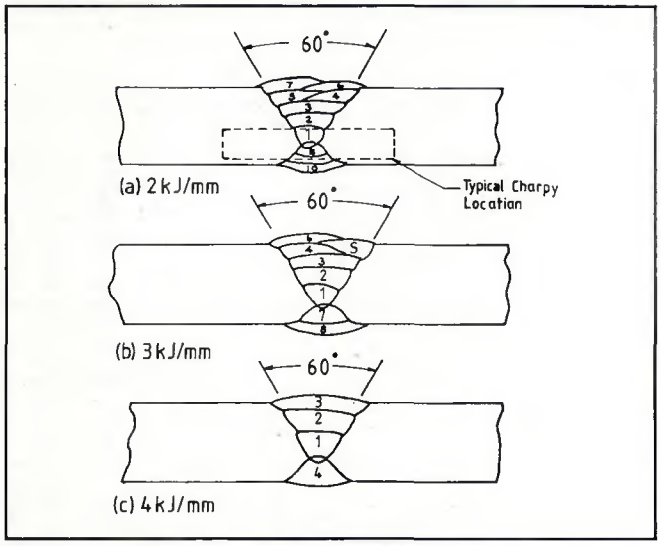

Fig. 1—Joint design preparation, pass sequence and Charpy specimen location for the submerged-arc welds

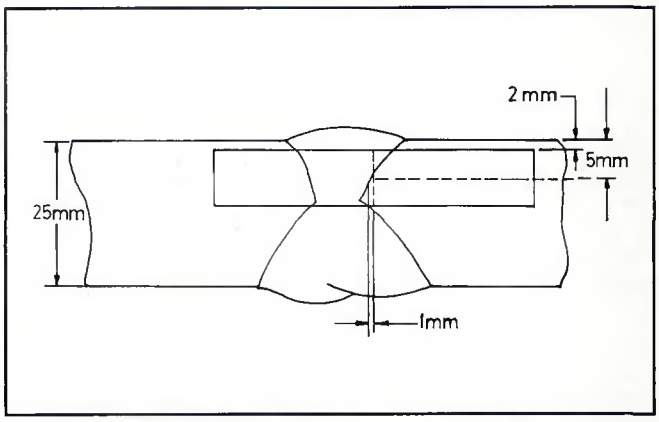

Fig. 2—Schematic diagram showing position of HAZ Charpy specimen, notched through thickness, 1 mm from the fusion line

merged arc welding consumables for HY 80/100 steels (Ref. 12).

Two series of submerged arc welds (Series A and Series B) were made using electrode/flux combinations approved for welding HY 80 at energy inputs less than or equal to 4 kJ/mm (102 kJ/in.). The two electrodes used were both 100S-1 (AWS EM2) classification, and the two fluxes were highly basic. The consumables, weld identifications, and welding parameters are listed in Table 3. The ranges of energy inputs employed were in accordance with the limits specified for HY 80 steels in the current military standard for HY 80/100 submarine construction (Ref. 13). Single-V joint design preparations were used with a 60-deg included angle and a 6- to 8-mm (0.24- to 0.31-in.) root face, to accommodate increasing energy input. Figure 1 shows the joint design preparation, pass sequence and Charpy test specimen location. The welds were air carbon arc back gouged on the second side prior to deposition of the final passes. All welding was done parallel to the plate rolling direction.

To evaluate the microstructure and mechanical properties of both as-welded and stress-relieved conditions, one half of each weld from Series A was subjected to a PWHT for 1 h at 600°C (1112°F) for stress relieving (SR). All the welds were inspected by x-ray radiography prior to machining mechanical test specimens.

Mechanical Testing and Metallography

The tensile properties were determined from all-weld-metal specimens for the Series A and B as-welded condition and the Series A stress-relieved condition. Charpy impact transition curves were generated for each test condition, including both weld metal and the CGHAZ regions. The specimens were notched through-thickness at the weld centerline and the CGHAZ 1 mm (0.04 in.) from the fusion line on the back gouged side of each weldment, as shown in Figs. 1A and 2, respectively.

The microstructures of the weld metal and the CGHAZ were identified and characterized using optical and scanning electron microscopy (SEM) for both the as-welded (AW) and the stress-relieved (SR) conditions. The specimens were prepared by standard metallographic techniques and subsequently etched in 2% nital to reveal the overall structure and in 4% picral for details of secondary microconstituents, M-A and/or carbides. Point counting was performed on the last as-deposited weld bead to determine the percentage of acicular ferrite (AF), grain boundary ferrite (GF), ferrite with second phase (FS) (aligned FS(A) and nonaligned FS(N)), and polygonal ferrite (PF) in accordance with current IIW recommendations (Ref. 14). Transmission electron microscopy was used to study copper precipitation in selected samples, using a two-stage carbon extraction replica technique. Energy dispersive x-ray analysis was used to determine the precipitate compositions.

Fractured surfaces of selected Charpy

Table 2—Mechanical Property Requirements for HSLA Submerged Arc Weld Metals

Yield strength	565 MPa min
Reduction in area	50% min
Elongation	20% min
Charpy impact energy	81 J at −18°C 47 J at −50°C

Table 3—Submerged Arc Welding Consumables and Parameters

Series	Weld No.	Energy Input, kJ/mm	Electrode/Flux Combination	Current, A	Wire Feed Speed, mm/s	Travel Speed, mm/s
A	SA20	2	Electrode A	450	55.0	7.8
	SA30	3	100S1 (EM2)	500	61.2	5.9
	SA30	4	Basic flux	570	76.2	5.1
			B.I. = 3.0*			
B	SA21	2	Electrode B	450	55.0	7.8
	SA31	3	100S1 (EM2)	500	61.2	5.9
	SA41	4	Basic flux	570	76.2	5.1
			B.I. = 2.7*			

Note: a) voltage setting—35 V; b) electrode extension—32 mm; c) preheat temperature—93°C; d) interpass temperature—149°C; e) electrode diameter—2.4 mm.
*Basicity index was provided by manufacturer.

Table 4—Chemical Composition of Submerged Arc Welds

Series	Weld No.	Element wt-%												
		C	Mn	Si	S	P	Ni	Cr	Mo	Al	Cu	N	O	Pcm
A	SA20	0.06	1.16	0.37	0.005	0.010	1.67	0.28	0.32	0.015	0.27	0.0086	0.0307	0.21
	SA30	0.05	1.14	0.37	0.005	0.010	1.43	0.27	0.29	0.015	0.41	0.0090	0.0282	0.20
	SA40	0.06	1.05	0.35	0.005	0.010	1.30	0.34	0.29	0.015	0.53	0.0109	0.0259	0.21
B	SA21	0.05	1.11	0.35	0.003	0.007	1.52	0.27	0.28	0.010	0.48	0.0094	0.0310	0.20
	SA31	0.05	1.13	0.35	0.003	0.007	1.32	0.24	0.28	0.010	0.40	0.0095	0.0274	0.19
	SA41	0.05	1.08	0.35	0.003	0.007	1.28	0.35	0.28	0.010	0.58	0.0094	0.0221	0.20

Note: For all weld metals, Nb = 0.020. Pcm (%) = C + Si/30 + Mn/20 + Cu/20 + Ni/60 + Cr/20 + Mo/15 + V/10 + 5 B.

Table 5—Chemical Composition of Welding Electrodes

	C	Mn	Si	S	P	Ni	Cr	Mo	Al	Cu
Electrode A 100S-1	0.08	1.64	0.30	0.008	0.007	1.74	0.08	0.28	0.021	0.02
Electrode B 100S-1	0.07	1.57	0.52	0.004	0.004	1.86	0.03	0.28	0.009	0.06

specimens were examined in a SEM to evaluate the cleavage fracture features for specimens containing the CGHAZ region. Microhardness measurements were made in the vicinity of the Charpy notches for both weld metal and CGHAZ regions using a diamond pyramid indenter with a 500-g load.

Results

Weld Metal Chemistry

The chemical compositions from the root region (Charpy position, Fig. 1) of the submerged arc welds and the corresponding electrode chemistries are presented in Tables 4 and 5, respectively. Only slight differences in chemistry were observed between the Series A and B welds. The higher Cu in the Series B welds was attributed to the copper coating of Electrode B. Variations in weld chemistry within each series reflect the increase of dilution as a result of higher energy inputs. The dilution ranged from about 30% for the 2-kJ/mm (51 kJ/in.) energy inputs to 65% for the 4-kJ/mm energy inputs. This was calculated geometrically for the back gouged side of the weldments. The primary differences in weld metal composition within each series are the increase in copper and chromium and the decrease in nickel and oxygen with increasing energy input. The reduction in oxygen should relate to a lower volume fraction of inclusions (Ref. 15).

Weld Metal Mechanical Properties

The results from weld metal Charpy impact testing are presented in Fig. 3 and Table 8. All welds exceeded the targeted toughness requirements of 47 J at −50°C (−58°F) and 81 J at −18°C (0°F) in the as-welded condition. In both Series A and B, the 4-kJ/mm welds had consistently higher notch toughness at temperatures below −40°C (−40°F). For the stress-relieved condition (Fig. 3A), only the 2-kJ/mm weld met the notch toughness requirements. The transition curves for the 3- and 4-kJ/mm (76- and 102-kJ/in.) welds were shifted to higher temperatures. All as-welded specimens exhibited full ductile behavior at the 20°C (68°F) impact testing temperature. In the stress-

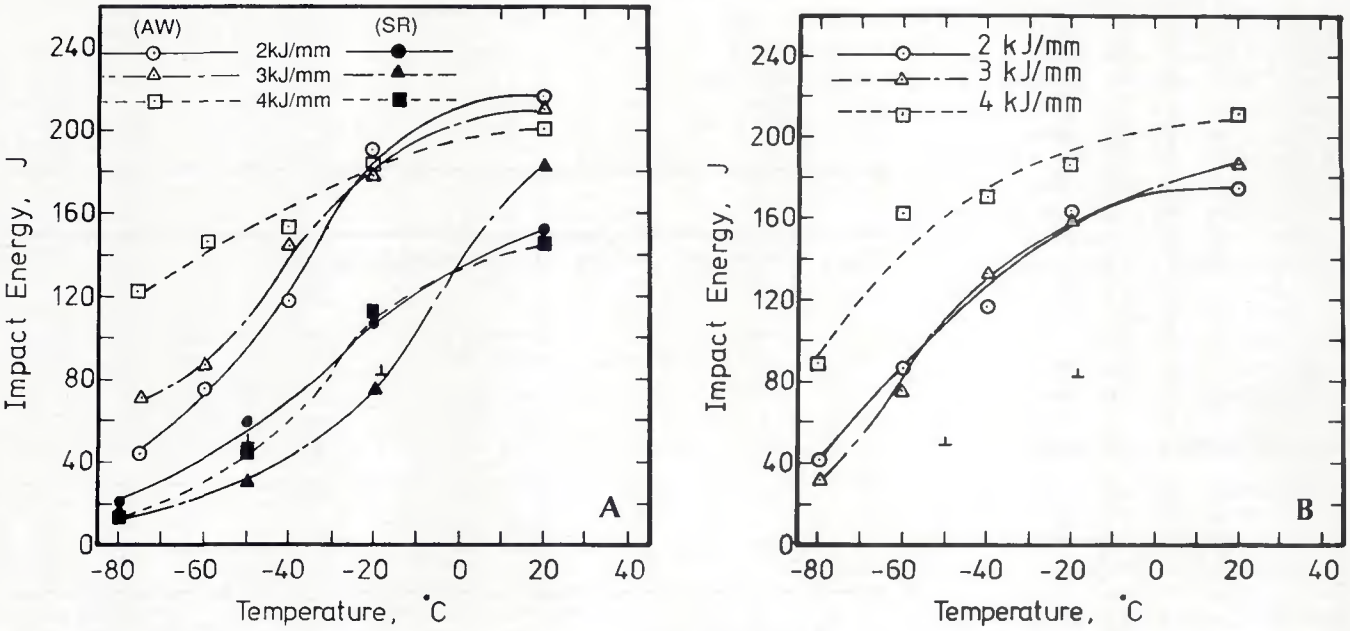

Fig. 3—Charpy transition curves for submerged arc weld metals. A—Series A; B—Series B

relieved condition, fully ductile behavior was not observed at the 20°C test temperature.

The tensile properties of the experimental welds are listed in Table 6. In general, there was no significant difference in the tensile properties between the Series A and B welds in the as-welded condition. All welds, with the exception of weld SA40 (AW), met or exceeded the minimum yield strength requirement of 565 MPa (81.9 ksi). A marked decrease in yield strength with increasing energy input was observed for both Series A and B welds. There was, however, a significant increase in yield strength observed in the Series A welds after stress relieving. This was most pronounced at the higher energy inputs (3 and 4 kJ/mm), where increases of 83 and 135 MPa (12,040 and 19,600 psi) occurred (13% and 24%, respectively), as shown in Table 6. As indicated in Table 7, only a slight decrease in microhardness with increasing energy input was observed for both Series A and B welds in the as-welded condition. All welds exceeded the percent elongation and reduction of area requirements in both the as-welded and stress-relieved conditions.

Table 6—Tensile Properties of Submerged Arc Weld Metals

Weld No.	Yield Strength, MPa		Ultimate Strength, MPa		Elongation, %		Reduction in area, %	
	AW	(SR)	AW	(SR)	AW	(SR)	AW	(SR)
SA20	658	(670)	714	(734)	27	(32)	72	(72)
SA30	604	(687)	698	(767)	25	(28)	72	(68)
SA40	564	(706)	699	(772)	24	(25)	63	(66)
SA21	669		750		27		72	
SA31	603		733		25		72	
SA41	565		709		29		74	

Note: AW—as welded; (SR)—stress relieved.

Table 7—Microhardness Results of HSLA 80 Weldments

Weld No.	Heat Input, kJ/mm	DPH CGHAZ AW	DPH CGHAZ (SR)	DPH Weld Metal AW	DPH Weld Metal (SR)
SA20	2	276	(292)	255	(238)
SA30	3	265	(293)	251	(241)
SA40	4	249	(288)	243	(258)
SA21	2	273		247	
SA31	3	242		235	
SA41	4	236		231	

Note: AW—as welded; (SR)—stress relieved.

Weld Metal Microstructure

The weld metal microstructure in the root region (from which the Charpy specimens were taken) for the Series A and B welds contained as-deposited and reheated regions for the 2- and 3-kJ/mm welds. The proportion of as-deposited structure increased from approximately 30% for the 2-kJ/mm weldments to 90% for the 4-kJ/mm weldments. For the low-energy-input (2 kJ/mm) weld, ten passes were required to complete the joint, compared with only four passes for the high-energy input (4 kJ/mm) weld—Fig. 1A.

Representative optical and SEM micrographs of the as-deposited region of Series A and B welds are shown in Figs. 4 and 5. The SEM micrographs were used to determine dimensions of acicular ferrite and location of the secondary microphases. In general, the microstructure within the as-deposited region was composed predominantly of acicular ferrite with various proportions of grain boundary ferrite, ferrite with second phase and polygonal ferrite. These constituents are identified in Figs. 4A and 5A. In addition to the major transformation products, the presence of martensite-austenite (M-A) microphase between acicular ferrite laths and at grain boundaries was observed in all welds after etching in a 4% picral solution—Fig. 7A. The quantitative analysis of the weld metal microstructure is presented in Table 8. For both Series A and B welds, there was a slight decrease in the amount of acicular ferrite with energy input. Estimates of the size of acicular ferrite lath width were made. These measurements indicated that there was a slight increase in coarseness (lath width changing from 1–3 μm to 3–5 μm) as energy input increased from 2 to 4 kJ/mm. As indicated in Table 8, the slight decrease in acicular ferrite with energy input was accompanied by an increase in total amount of the minor constituents,

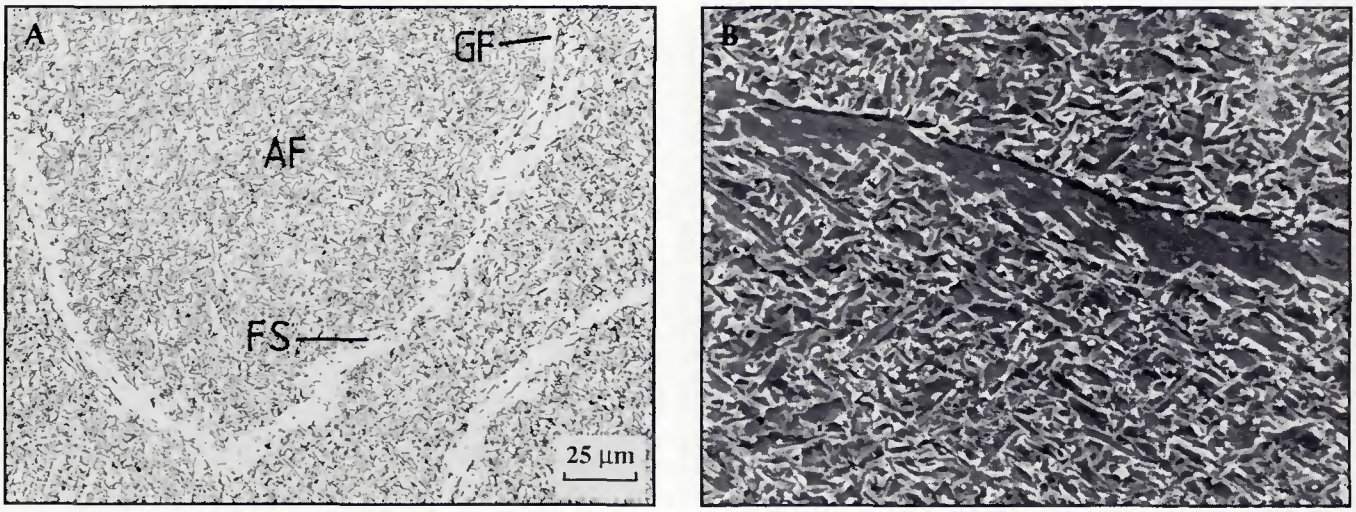

Fig. 4—Microstructure of the as-deposited region of weld SA20 (Series A) deposited at 51 kJ/in. A—Optical; B—SEM

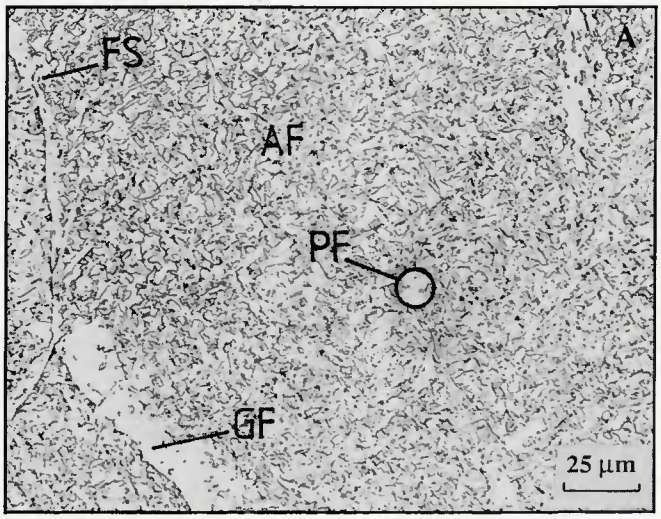

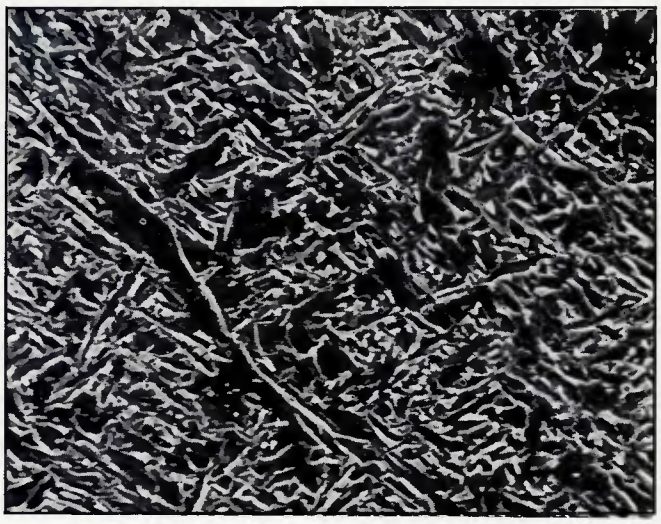

Fig. 5 — Microstructure of the as-deposited region of weld SA41 (Series B) deposited at 102 kJ/in. A — Optical; B — SEM

i.e., grain boundary ferrite, ferrite with second phase and polygonal ferrite. The typical microstructure of the reheated weld metal region is shown in Fig. 6. The structure consisted of acicular ferrite delineated by grain boundary ferrite and ferrite with second phase for both Series A and B welds. Stress relieving of Series A welds did not change the overall microstructure. There was, however, an increase in the proportion of carbides, shown in Fig. 7.

Energy dispersive x-ray analysis was performed on extraction replicas prepared from the Series A welds deposited at 2- and 4-kJ/mm energy inputs and revealed the presence of 10- to 20-mm diameter Cu precipitates for the as-welded and stress-relieved conditions — Fig. 8. The size of the precipitates was similar for both the 2- and 4-kJ/mm welds. The dispersion of precipitates was not uniform throughout the welds, but varied significantly between individual grains. Indeed, some grains were devoid of precipitates, while others contained precipitates as a result of Cu microsegregation. In addition to Cu precipitates, some iron carbides were observed in the as-welded condition in both the 2- and 4-kJ/mm welds.

Stress relieving of the welds resulted in an increase in the proportion of Cu precipitates compared with the as-welded condition, particularly for the 4-kJ/mm weld — Figs. 8B–D. After stress relieving, no difference in Cu precipitate density could be discerned between the 2- and 4-kJ/mm welds. There was, however, an increase in the proportion of iron carbide precipitates observed, as shown in Fig. 8.

Table 8—Percentage of Microstructural Constituents of Submerged Arc Weld Metals for Series A and B

	% of Constituents				
Weld No.	AF	GF	FS(A)	FS(N)	PF
SA20	79	15	2	2	2
SA30	85	9	1	2	3
SA40	75	12	2	4	7
SA21	73	16	2	4	5
SA31	79	10	2	2	7
SA41	67	9	7	9	8

Note: AF — acicular ferrite; GF — grain boundary ferrite; FS(A) — ferrite with second phase (aligned); FS(N) — ferrite with second phase (non-aligned); PF — intragranular polygonal ferrite.

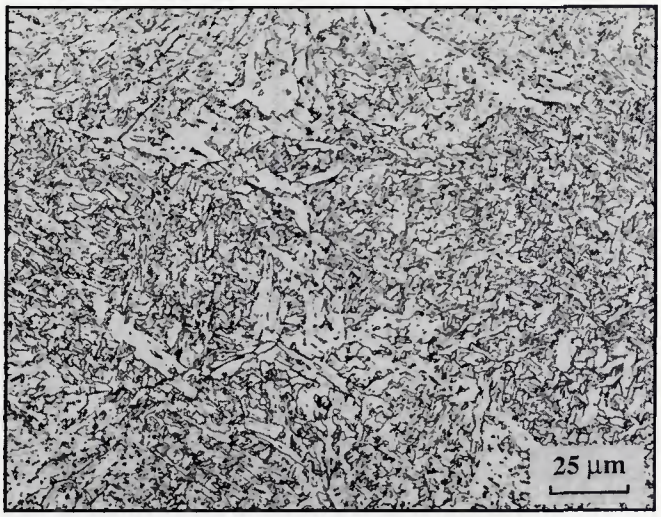

Fig. 6 — Microstructure of reheated weld metal region in submerged arc weld deposited at 51 kJ/in.

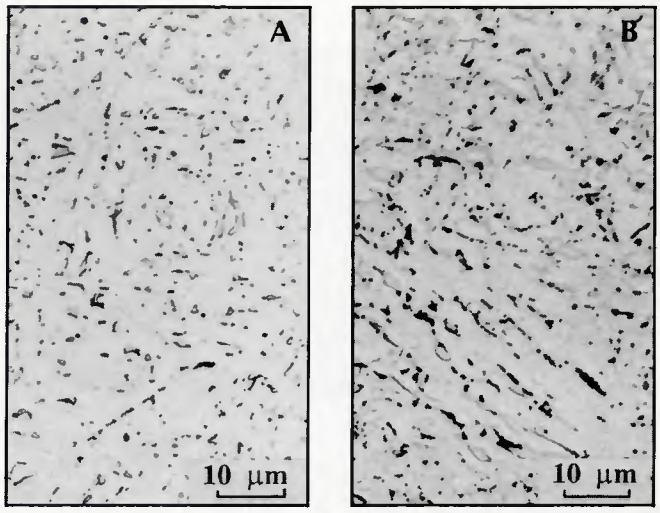

Fig. 7 — Microstructure of as-deposited region in weld SA40 etched in a 4% picral solution. A — M-A microphases in as-welded condition; B — carbides after stress relieving

Table 9—Summary of Weld Metal and CGHAZ Notch Toughness Results

Series	Heat Input, kJ/mm	Weld Metal, J (AW) −50°C	Weld Metal, J (AW) 20°C	Weld Metal, J (SR) −50°C	Weld Metal, J (SR) 20°C	CGHAZ, J (AW) −50°C	CGHAZ, J (AW) 20°C	CGHAZ, J (SR) −50°C	CGHAZ, J (SR) 20°C
	2	96	216	58	157	107	267	198	235
A	3	110	210	30	182	85	277	103	230
	4	152	200	45	147	62	271	44	206

Note: Base material impact energy at −50°C—240 J as received; 325 J stress-relieved. AW—as welded. (SR)—stress relieved.

In addition, in both the as-welded and stress-relieved conditions, no alloy carbides or niobium carbonitrides were observed.

CGHAZ Notch Toughness

Charpy impact transition curves generated for the CGHAZ (notched through-thickness 1 mm/0.04 in. from the fusion line) of the Series A weldments are shown in Fig. 9. Increasing energy input resulted in a displacement of the Charpy transition curves to higher temperatures. All welds in the as-welded condition exceeded the impact requirements. For the Series A welds, stress relieving improved the notch toughness of the 2- and 3-kJ/mm welds and reduced the toughness of the 4-kJ/mm weld. The results are summarized in Table 8. The microhardness of the CGHAZ region adjacent to the fusion line increased for all three energy inputs, as shown in Table 7.

CGHAZ Microstructure

The as-welded microstructures of the CGHAZ adjacent to the fusion line are shown in Figs. 10 and 11 for the 2- and 4-kJ/mm energy inputs. For the lowest 2-kJ/mm energy input (Figs. 10A and B), the microstructure consisted of a mixture of bainite with some regions of low-carbon martensite. At the higher energy inputs of 3 and 4 kJ/mm (Figs. 11A and B), a predominantly coarse upper bainite structure was formed. The bainite consisted of packets of parallel bainitic-ferrite laths separated by islands of M-A microphases—Fig. 12A. The bainitic packets increased in size with increasing energy input. The M-A constituent was decomposed to carbide after stress-relieving, as shown in Fig. 12B.

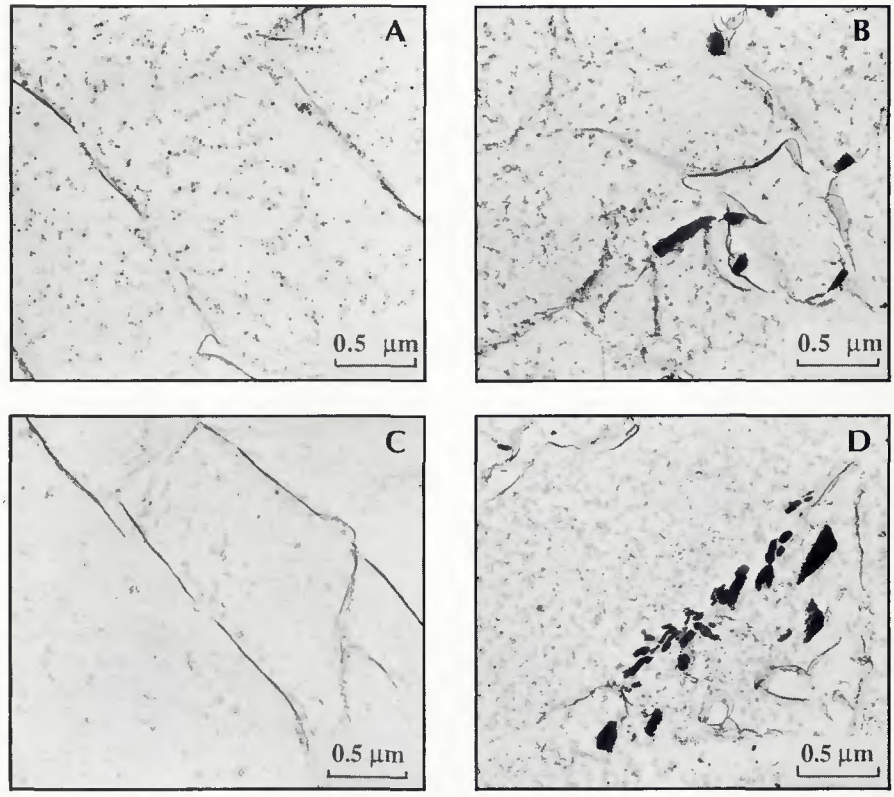

Fig. 8—Transmission electron micrographs of carbon extraction replicas showing precipitates in the as-deposited region of submerged arc weld metals deposited at 51 kJ/in. (weld SA20) and 102 kJ/in. (weld SA40). A—Weld SA20, as welded; B—Weld SA20, stress relieved; C—Weld SA40, as welded; D—Weld SA40, stress relieved

Discussion

The present studies on submerged arc welding of precipitation-hardened HSLA 80 have shown that the weld metal notch toughness (47 J at −50°C and 81 J at −18°C) and tensile property requirements can be achieved in the as-welded condition using the commercially available HY 80 consumables for the energy input range of 2 to 4 kJ/mm. There was, however, a significant decrease in weld metal yield strength and an increase in notch toughness associated with the highest 4 kJ/mm energy input. Stress relieving (at 600°C for 1 h) reduced the weld metal notch toughness and increased the yield strength. After stress relieving, only the 2 kJ/mm weld exceeded the notch toughness requirements.

The CGHAZ notch toughness in the as-welded condition decreased with increasing energy input, although in all cases the toughness requirements were met or exceeded. Stress-relieving decreased the CGHAZ notch toughness of the 4-kJ/mm weldment below the target requirements.

In general, these results can be explained in terms of the microstructural characteristics of weld metal and CGHAZ regions affected both by increasing energy input and by stress relieving.

Weld Metal Properties and Microstructure

The high proportion of acicular ferrite (AF) combined with a low oxygen plus sulfur content of 220–315 ppm (reflecting a low inclusion volume fraction (Ref. 15)) were the primary microstructure features contributing to the superior low temperature notch toughness of the welds. Acicular ferrite weld metals consist of highly dislocated, low-aspect-ratio (4:1) ferrite laths, typically 1–3 μm wide, separated by high-angle grain boundaries. Acicular ferrite provides optimum resistance to cleavage crack propagation because cracks must re-initiate at the closely spaced high-angle boundaries. A relationship has been proposed showing that the amount of weld metal AF is maximized for Pcm carbon equivalent levels in the range of 0.17 to 0.23 (Ref. 16). A comparison of the calculated hardenabilites using

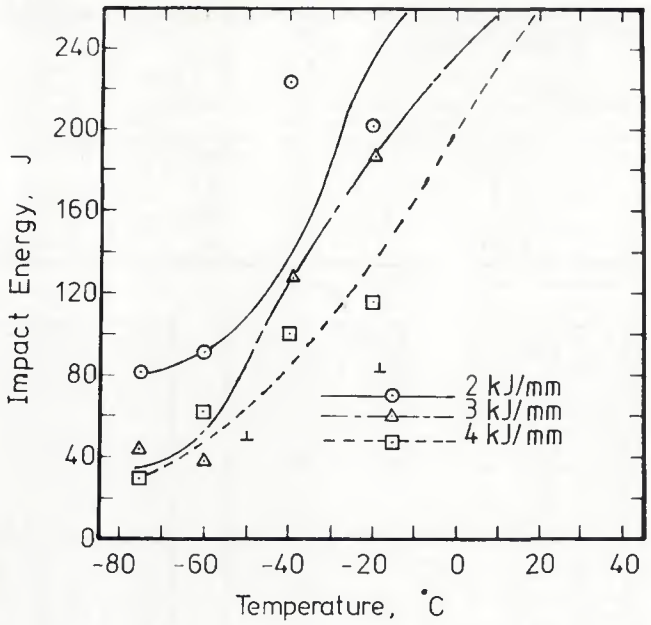

Fig. 9—Charpy transition curves of the CGHAZ notched 1 mm from the fusion line

the Pcm (Table 4) shows that all weld metal compositions were within this optimum range. In addition, the oxygen levels (Table 4) were in the optimum range (200–400 ppm) where, as oxide inclusions, they could act as nucleation sites for AF formation (Ref. 17).

In the as-welded condition, there was a trend toward higher notch toughness with increasing energy input for both Series A and B welds (Fig. 3), despite coarsening of the microstructure at the highest energy input. A similar trend was observed by Jesseman and Schmid (Ref. 7). In general, higher notch toughness may be expected at low energy inputs (2 kJ/mm) because of the high proportion of fine reheated (several welds beads) and as-deposited weld metal structure. The precipitation of copper in the reheated weld metal (Fig. 8A) may be an important factor in reducing the toughness at low energy inputs. The higher strength of the 2-kJ/mm weld (Table 6) reflects the likely precipitation strengthening of copper. Further studies using Gleeble simulation techniques are needed to clarify the role of copper precipitation in reheated regions of the weld metal and its effect on strength and toughness.

Stress relieving of the Series A weld metals resulted in a loss of notch toughness. The Charpy transition curves were shifted to higher temperatures and failed to meet the toughness requirement at −50°C for the 3- and 4-kJ/mm energy inputs. In the stress-relieved condition, the decrease in notch toughness was accompanied by an increase in yield strength. This increase in yield strength resulted primarily from increased copper precipitation—Fig. 8. The increase in yield strength was considerably less for the 2-kJ/mm weld compared with the 4-kJ/mm weld (Table 6), which is consistent with the lower level of copper precipitation observed in the 4-kJ/mm weld in the as-welded condition.

In addition, an increase in iron carbide precipitation after stress relieving in the 2-, 3-, and 4-kJ/mm Series A welds also contributed to the loss in notch toughness. Embrittlement resulting from increased iron carbide precipitation after

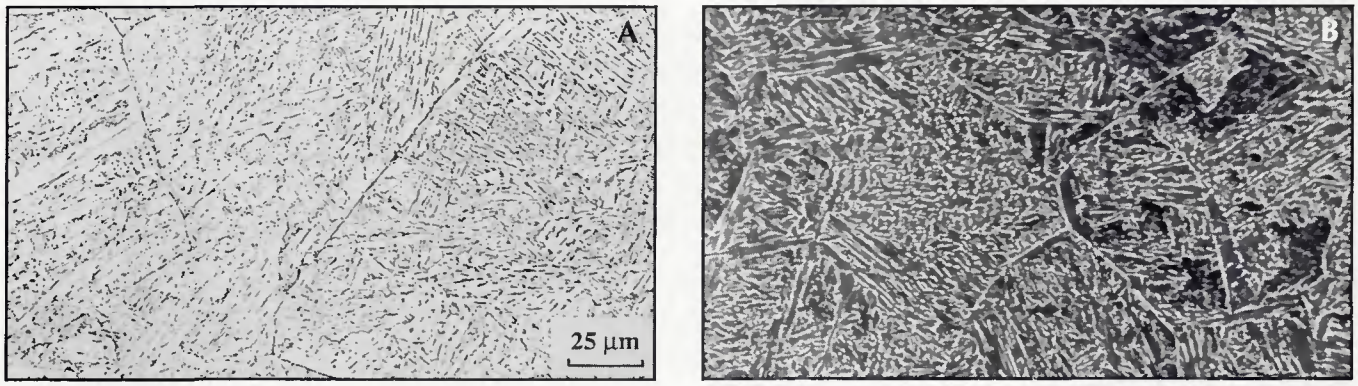

Fig. 10—Microstructure of the CGHAZ region, showing bainite and low carbon martensite for a 51-kJ/in. energy input. A—Optical; B—SEM

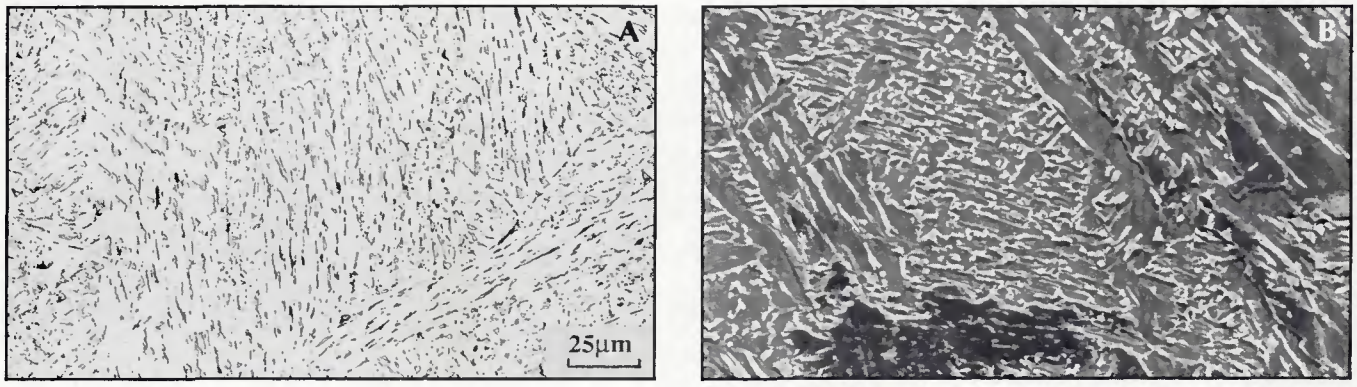

Fig. 11—Microstructure of the CGHAZ region (coarse upper bainite) for a 102-kJ/in. energy input. A—Optical; B—SEM

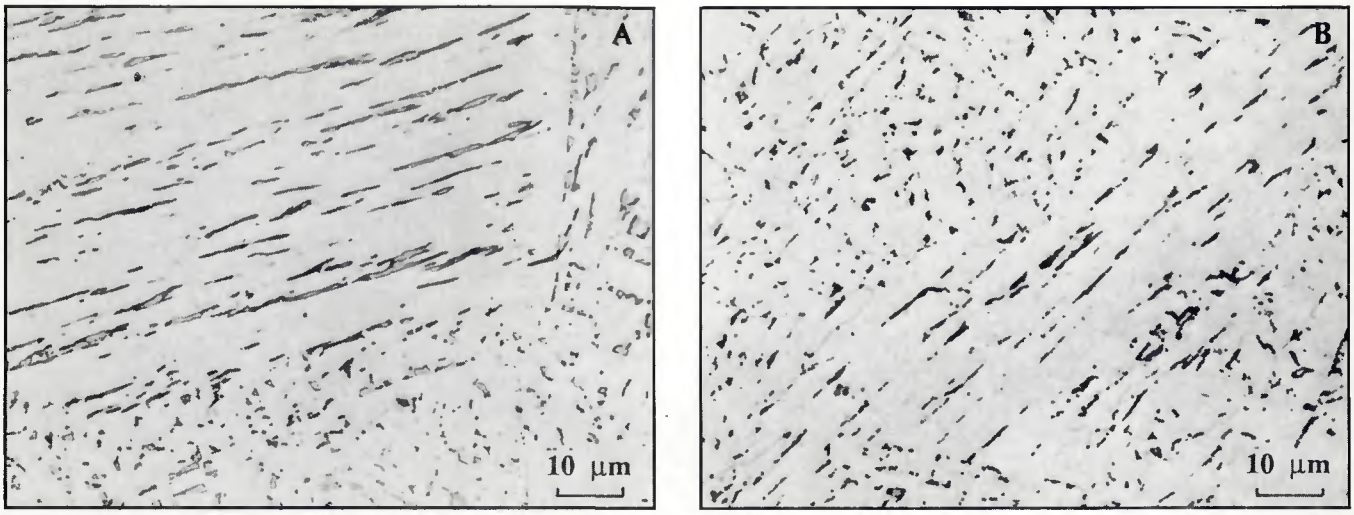

Fig. 12 — Micrographs of the CGHAZ deposited at 102 kJ/in. Etched in 4% picral solution to reveal microphases of M-A microconstituents and carbides. A — As welded; B — stress relieved

stress relieving has also been reported by Braid and Gianetto (Ref. 18) for C-Mn-Ni shielded metal arc welds. Optical and transmission electron microscopy revealed an increased proportion of iron carbides in the stress-relieved condition, as shown in Figs. 7 and 8. This was partly associated with decomposition of M-A microphases, which offsets normal softening of the weld metal microstructure after stress relieving.

CGHAZ Properties and Microstructure

Although the CGHAZ Charpy results in the as-welded condition exceeded the target values, a general trend to decreasing notch toughness was observed for increasing energy input. This was caused by two factors: 1) the increased energy input results in a larger proportion of CGHAZ being sampled; and 2) an overall coarsening of the HAZ microstructure from the longer cooling times of the higher-energy-input welds. In order to explain the change in the notch toughness, the proportions of the microstructural regions at the notch of the Charpy impact test specimen must be considered. For the CGHAZ impact test, the notch is located next to the fusion line (Fig. 2), therefore sampling several microstructural regions, including weld metal, CGHAZ and base metal. Thus, the measured notch toughness includes the sum of the individual contributions of these regions (Refs. 19, 20). The work of Satoh, *et al.* (Ref. 20), has shown that as the proportion of an embrittled region increases, the toughness approaches that of the lowest toughness region, for Charpy and CTOD testing.

At the low energy input (2 kJ/mm) the CGHAZ region is small and represents only about 10–20% of the total fractured path; therefore, the high toughness contributions of the AF weld metal and fine-grained polygonal ferrite base metal result in superior low temperature toughness, measured by the CGHAZ impact test. At the higher energy input, 4 kJ/mm, the CGHAZ represents about 30–50% of the total fracture path, and the measured notch toughness is lower.

In addition, the microstructure of the CGHAZ changes with increasing energy input. In this study, the CGHAZ changed from a fine bainite with regions of low-carbon martensite at 2 kJ/mm to a coarse upper bainite at 4 kJ/mm, as discussed above. The presence of low-carbon martensite in the 2-kJ/mm CGHAZ, which was difficult to distinguish in the optical microscope, was confirmed using SEM, which revealed the presence of step-like facets 5 to 10 μm wide, as shown in Fig. 13A. At 4 kJ/mm, the CGHAZ was a band containing large cleavage facets 40 to 80 μm wide — Fig. 13B. This coarse upper

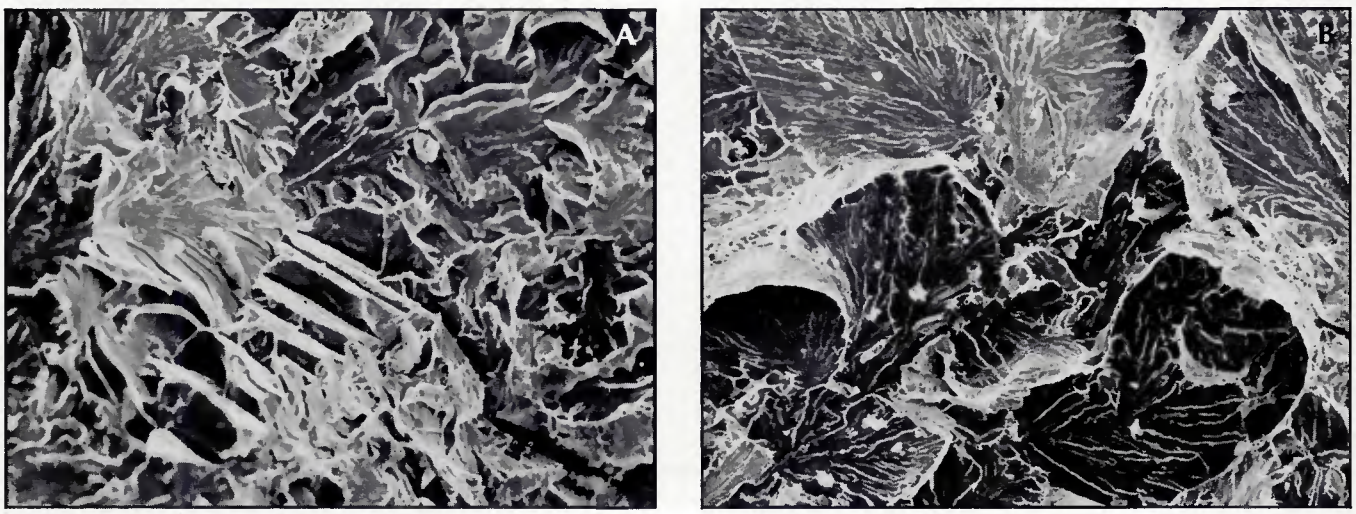

Fig. 13 — SEM fractographs of fractured HAZ Charpy specimens. A — Fractograph of 51-kJ/in. Charpy specimen showing cleavage facets corresponding to the mixed bainite (large facets) and low-carbon martensitic (step-like facets) microstructure. B — Cleavage facets of the 102-kJ/in. Charpy specimen corresponding to the coarse upper bainite microstructure

bainitic structure has very low cleavage fracture resistance (Ref. 10) and was mainly responsible for the overall reduced toughness exhibited in the CGHAZ impact test (Fig. 9) at 4 kJ/mm. The reduction in toughness contributed by the CGHAZ region was partially offset by the improved toughness of the weld metal region exhibited (Fig. 9) at 4 kJ/mm.

Stress relieving increased the HAZ notch toughness of the 2- and 3-kJ/mm welds but lowered the toughness of the 4-kJ/mm welds. These results can also be explained on the basis of the proportions of the microstructural regions in the fracture path, despite the embrittlement of the HAZ (reflected by the higher microhardness, Table 7) even at low-energy inputs as a result of precipitation of copper and iron carbides. At 2 and 3 kJ/mm, CGHAZ occupies only 10–30% of the fracture path; therefore, the increased toughness is attributable to the higher toughness of the base metal region after stress relieving. At 4 kJ/mm, the decrease in toughness was attributed to the increased proportion of CGHAZ (30–50%) taking part in the fracture and the further embrittlement of the coarse bainite microstructure.

Conclusions

1) The series of submerged arc welds deposited with commercially available welding consumables for the energy input range of 2–4 kJ/mm exceeded the notch toughness requirements of 47 J at −50°C and 81 J at −18°C in the as-welded condition.

2) The weld metal notch toughness properties were attributed to a high proportion of acicular ferrite microstructure combined with a low O + S content.

3) The superior low-temperature notch toughness of the highest (4 kJ/mm) energy input welds was related to the lower yield strength, compared to the multipass 2- and 3-kJ/mm welds. The tendency to lower yield strength with increasing energy input was caused by a slight coarsening of the weld metal microstructure and a reduction in copper precipitation hardening at the highest energy input.

4) A loss of notch toughness and accompanying increase in yield strength was observed after stress relieving of the Series A welds. In general, this was attributed to an increase in copper and carbide precipitation.

5) In the as-welded condition, the decrease in notch toughness of the CGHAZ specimens as the energy input was increased resulted from the following: a) an increasing proportion of the CGHAZ taking part in the fracture; and b) a change in microstructure of the CGHAZ from low-carbon martensite/bainite to coarse upper bainite.

6) In the stress-relieved condition, there was an improvement in the CGHAZ specimen notch toughness for the 2- and 3-kJ/mm weldments. This was related to the improved toughness of the base metal, which represented a significant proportion of the fracture path. For the 4-kJ/mm weldment, the increased proportion of CGHAZ in the fracture path resulted in lower toughness.

Acknowledgments

The authors would like to thank Mr. D. Dolan for the preparation of the experimental welds, Miss J. Ng-Yelim for the characterization and evaluation of weld precipitates by electron microscopy, and Dr. J. Bowker for useful discussions.

References

1. McGrath, J. T., Gianetto, J. A., Orr, R. F., and Letts, M. W. 1987. Some factors affecting the notch toughness properties of high strength HY80 weldments. *Canadian Metallurgical Quarterly* 25(4):349–356.

2. Franke, G. L. 1985. Submerged arc welding of high yield strength steel. Welding for challenging environments. *Proc. of the Int. Conf. on Welding for Challenging Environments:* 283–291. Toronto: Pergamon Press.

3. Jesseman, R. J., and Murphy, G. J. 1983. Mechanical properties and precipitation hardening response in ASTM A710 Grade A and A736 alloy steel plates. *Proc. Int. Conf. on Technology and Applications of High Strength Low Alloy (HSLA) Steels Philadelphia:* 655–666. Metals Park, Ohio: ASM.

4. Wilson, A. D. 1987. High strength, weldable precipitation aged steels. *Journal of Metals* March: 36–38.

5. Krishnadev, M. R. 1984. Development and characterization of a new family of HSLA steels. *HSLA Steels, Technology and Applications:* 129–148. Metals Park, Ohio: ASM.

6. Montemarano, T. W.; Sack, B. P.; Gudas, J. P.; Vassilaros, M. G.; and Vanderveldt, H. H. 1986. High strength low alloy steels in naval construction. *Journal of Ship Production* 2(3):145–162.

7. Jesseman, R. J., and Schmid, G. C. 1983. Submerged arc welding a low-carbon copper-strengthened alloy steel. *Welding Journal* 62(11):321-s to 330-s.

8. Kvidahl, L. D. 1985. An improved high yield strength steel for shipbuilding. *Welding Journal* 64(7):42–48.

9. Ferree, S. E. 1987. Flux cored arc welding of high strength steels. *Australian Welding Journal* 32(1):5–13.

10. Krishnadev, M. R., McGrath, J. T., Bowker, J. T., Dionne, S., and Lassravini, A. 1987. HAZ microstructure and toughness of precipitation strengthened HSLA steels and conventional HY-grade high strength steels. *Proc. AIME Int. Symposium on Welding Metallurgy of Structural Steels,* Denver, Colo. Ed. J. Y. Koo: 137–155. Warrendale: AIME.

11. Abeln, S. P., Huppi, G. S., Brown, E. L., Matlock, D. K., and Edwards, G. R. 1987. The microstructure and properties of selected high strength ferritic weld metals. *Proc. of the Eighteenth Annual Technical Meeting of the International Metallographic Society:* 99–114. Columbus: IMS; Metals Park: ASM.

12. U.S. Dept. of Defense. 1983. Military Standard MIL-E-23765/2C (SH).

13. U.S. Dept. of Defense. 1981. Military Standard MIL-STD-1688 (SH).

14. Pargeter, R. J., and Dolby, R. E. 1985. Guidelines for Classification of Ferritic Steel Weld Metal Microstructural Constituents Using the Light Microscope. IIW Doc. IX-1377-85.

15. Liu, S., and Olson, D. L. 1986. The role of inclusions in controlling HSLA steel weld microstructures. *Welding Journal* 65(6):139-s to 149-s.

16. Grong, O., and Matlock, D. K. 1986. Microstructural development in mild and low alloy steel weld metals. *Int. Metals Review* 31(1):27–48.

17. Cochrane, R. C., and Kirkwood, R. P. 1978. The effect of oxygen on weld metal microstructure. *Trends in Steel and Consumables for Welding.* Paper 35, The Welding Institute: 103–121.

18. Braid, J. E. M., and Gianetto, J. A. 1985. The effects of PWHT on the toughness of shielded metal arc weld metals for use in Canadian offshore fabrication. *Proc. of the Int. Conf. on Welding for Challenging Environments:* 145–155. Toronto: Pergamon Press.

19. Pisarski, H. G., and Pargeter, R. J. 1984. Fracture toughness of weld heat affected zones (HAZs) in steels used in constructing offshore platforms. *Proc. of the Int. Conf. on Welding in Energy Related Projects:* 415–428. Toronto: Pergamon Press.

20. Satoh, K., Toyoda, M., and Minami, F. 1987. Thickness effect in fracture toughness of steel welds. IIW Doc. X-1135-87.